ADVANCES IN ATMOSPHERIC SCIENCES
大气科学进展

EARLY ONLINE RELEASE

The DOI for this manuscript is doi: 10.1007/s00376-017-8089-8.

Impacts of the Autumn Arctic Sea Ice on the Intraseasonal Reversal of the Winter Siberian High

Zhuozhuo LÜ[*1,2,3], Shengping HE[4], Fei LI[5], and Huijun WANG[6,2,1]

[1]*Nansen-Zhu International Research Centre, Institute of Atmospheric Physics, Chinese Academy of Sciences, Beijing* 100029, *China*

[2]*Climate Change Research Center, Chinese Academy of Sciences, Beijing* 100029, *China*

[3]*University of Chinese Academy of Sciences, Beijing* 100049, *China*

[4]*Geophysical Institute, University of Bergen and Bjerknes Centre for Climate Research, Bergen* 5007, *Norway*

[5]*NILU-Norwegian Institute for Air Research, Kjeller* 2007, *Norway*

[6]*Collaborative Innovation Center on Forecast and Evaluation of Meteorological Disasters/Key Laboratory of Meteorological Disaster, Ministry of Education, Nanjing University of Information Science and Technology, Nanjing* 210044, *China*

(Received 16 April 2018; revised 14 August 2018; accepted 18 September 2018)

ABSTRACT

During 1979--2015, the intensity of the Siberian high (SH) in November and December--January (DJ) is frequently shown to have an out-of-phase relationship, which is accompanied by opposite surface air temperature and circulation anomalies. Further analyses indicate that

[*] Corresponding author: Zhuozhuo LÜ
Email: lvzhuozhuo16@mail.ucas.edu.cn

the autumn Arctic sea ice is important for the phase reversal of the SH. There is a significantly positive (negative) correlation between the November (DJ) SH and the September sea ice area (SIA) anomalies. It is suggested that the reduction of autumn SIA induces anomalous upward surface turbulent heat flux (SHF), which can persist into November, especially over the Barents Sea. Consequently, the enhanced eddy energy and wave activity flux are transported to mid and high latitudes. This will then benefit the development of the storm track in northeastern Europe. Conversely, when downward SHF anomalies prevail in DJ, the decreased heat flux and suppressed eddy energy hinder the growth of the storm track during DJ over the Barents Sea and Europe. Through the eddy--mean flow interaction, the strengthened (weakened) storm track activities induce decreased (increased) Ural blockings and accelerated (decelerated) westerlies, which makes the cold air from the Arctic inhibited (transported) over the Siberian area. Therefore, a weaker (stronger) SH in November (DJ) occurs downstream. Moreover, anomalously large snowfall may intensify the SH in DJ rather than in November. The ensemble-mean results from the CMIP5 historical simulations further confirm these connections. The different responses to Arctic sea ice anomalies in early and middle winter set this study apart from earlier ones.

Key words: Siberian high, Arctic sea ice, storm track, phase reversal

1. Introduction

Over the largest continent in the world, the Siberian high (SH) plays a key role in the Eurasian winter climate. It has been revealed that the strength of the East Asian winter monsoon (EAWM) is closely related to the formation and evolution of the SH, which often leads to cold-air outbreaks in East Asia (Ding and Krishnamurti, 1987; Ding, 1990; Wang and He, 2012b; He and Wang, 2013b). Cold winters and extreme weather events have been found to have occurred frequently during the last decade in Eurasia (Cattiaux et al., 2010; Guirguis et al., 2011; Tang et al., 2013). In January--February 2008, an unusual cold-air outbreak and freezing-rain event hit South China, causing a considerable number of casualties and heavy losses of property. Additionally, extreme low temperatures occurred over continental Eurasia during January--February 2012, when the SH index value reached its maximum since 1979 (Cohen et al., 2014; Wu et al., 2017).

Numerous studies have been conducted to investigate the characteristics and variabilities of the SH. Most early work focused on regional heat budgets and circulation anomalies related to the SH. It was suggested that strong radiative cooling, large-scale descending motion and heating in the upper troposphere all contribute to the formation and maintenance of the SH (Ding and Krishnamurti, 1987). Takaya and Nakamura (2005b) pointed out that the intraseasonal amplification of the SH is associated with a blocking ridge caused by a Rossby wave packet propagating in the upper troposphere from the Euro-Atlantic area to the Far East. They further identified two different types of upper-level blocking correlated with the intraseasonal amplification of the SH. One is the so-called Atlantic-origin wave train, which is primarily associated with eastward propagating quasi-stationary Rossby waves. And the other

is the westward Pacific-origin type (Takaya and Nakamura, 2005a). During the past several decades, many studies have been conducted with the aim to explore the relationships between the variability of the SH and the North Atlantic Oscillation/Arctic Oscillation (AO) (Thompson and Wallace, 1998). It has been shown that the SH is significantly correlated with the AO; that is, a negative-phase AO is concurrent with a stronger SH and cold surges (Gong et al., 2001; Park et al., 2011; He, 2015). However, some exceptions have been highlighted whereby the AO is not significantly correlated with the SH. Wu and Wang (2002) argued that the AO and SH may play relatively independent roles in the climate variabilities of East Asia. Hor et al. (2011) also found that the AO alone cannot account very well for the 2009/10 cold-air outbreak and its intraseasonal periodicity.

Recently, many studies have connected the variability of the midlatitude climate to cryospheric conditions, such as Arctic sea-ice cover and Eurasian snow cover (e.g., Wang and He, 2012a; Li et al., 2015; Wegmann et al., 2015; Ruggieri et al., 2016; Zhou, 2017). According to Overland et al. (2015), a high regional loss of sea ice is more important to the longitudinal connections between the Arctic and the midlatitudes than to the Arctic-wide zonal influence. Jung et al. (2014) also pointed that, when making medium-range and extended-range climatic predictions, the Arctic, especially the subpolar region, has stronger influences on the climate of eastern Europe, northern Asia, and northeastern Canada than the tropics. Recently, the so-called “warm Arctic--cold Siberia” (WACS) pattern, a well-known Arctic--midlatitude climatic phenomenon, has been revealed as the winter atmospheric response of the Northern Hemisphere to the rapid change in Arctic properties (Overland et al., 2011; Cohen et al., 2013;

Mori et al., 2014). Concerning the generation of the WACS pattern, the pioneering work by Honda et al. (2009) implied that enhanced ocean-to-atmosphere energy flux due to sea-ice loss over the Barents-- and Kara seas triggered a stationary Rossby wave. Subsequently, it tended to amplify the wintertime SH, causing cold anomalies over eastern Eurasia. In addition, the release of ocean heat induced a northward shift in cyclonic pathways under light ice conditions, which caused the WACS anomaly (Inoue et al., 2012). Several connections have also been uncovered for relatively fast atmospheric dynamics (daily to weekly) (Deser et al., 2007). Most studies agree that sea-ice loss impacts the climate in the midlatitudes primarily by modifying the boundary layer. Moreover, the impacts on delayed and remote atmospheric anomalies are more likely caused by preceding sea-ice reduction (Li and Wang, 2013; Huang et al., 2017). A leading of sea-ice concentration anomalies (ice leads atmosphere) provides a more skillful predictability of atmospheric variabilities during wintertime than a lagging (atmosphere leads ice) during other seasons (Wu and Zhang, 2010).

The above-mentioned studies mainly took the seasonally averaged (e.g., December--February) or extended winter (i.e., November--March) anomalies as the representation of winter signals. However, it is worth mentioning that one particular month was often inconsistent with other months in the averaged season (Seierstad and Bader, 2008; He and Wang, 2013a). Recently, an evident phase reversal of the SH between November and December--January (DJ) was revealed by Chang and Lu (2012). Specifically, in the winter of 1995, negative sea level pressure (SLP) anomalies extended widely north of 40° N in November, whereas they were replaced by a broad range of positive SLP anomalies in DJ (top

panel of Fig. 1a). A strikingly opposite situation also appeared in the ensuing year of 1996, with positive SLP anomalies in November and negative anomalies in DJ over Siberia (top panel of Fig. 1b). The surface air temperature (SAT) anomalies were inverted between November and DJ correspondingly (bottom panels of Figs. 1a and b). Chang and Lu (2012) suggested that such reversions of the SH may be related to the less frequent Pacific and Ural blocking during a positive AO period. However, questions remain on the physical mechanism of such an intraseasonal phase change. In this respect, based on Arctic--midlatitude interactions, we attempt to explain how the reversion happens.

2. Data and methods

The atmospheric data used in this study are from the National Centers for Environmental Prediction--National Center for Atmospheric Research (NCEP--NCAR) reanalysis dataset, covering the period from November 1979 to January 2016 (Kalnay et al., 1996). The variables used include monthly mean SLP, SAT, 850 hPa zonal and meridional wind (uv850), geopotential height at 500 hPa (Z500), 300 hPa zonal wind (u300), surface turbulent heat flux (SHF), and daily mean geopotential height at 250 hPa (Z250) and Z500. The monthly mean SHF from the European Centre for Medium-Range Weather Forecasts interim reanalysis (ERA-Interim) (Dee et al., 2011) is also used to verify the NCEP--NCAR SHF data. Here the SHF is defined as the sum of surface sensible and latent heat flux. The monthly sea-ice concentration is from the HadISST dataset (Rayner et al., 2003). The monthly mean Arctic sea-ice area (SIA, i.e., the concentrations multiplied by the area of corresponding grid cells with at

least 15% sea-ice concentration) is analyzed in this study. Daily mean snow depth data for 1979--2016 derived from ERA-Interim are also used.

Two indices are used in this paper: the Siberian high index (SHI) and the SIA index (SIAI). The SHI is defined as the area-averaged monthly mean SLP in the domain shown in Fig. 2 (40°--60°N, 70°--120°E; black box), which is consistent with the climatological center of the winter-mean SLP distribution over Eurasia (Zhao and Zhang, 2006; Wu et al., 2011). The SIAI is defined as the detrended September area-averaged SIA within the area (71°--81°N, 30°--150°E). The time series of both indices are normalized for comparability. Besides, the sign of the SIAI is reversed so that all regressions on the SIAI shown in this study correspond to the reduction in sea ice.

Representing the wave activity propagation, the three-dimensional wave activity flux (WAF) derived by Takaya and Nakamura (2001) is calculated to illustrate the energy flow between the Arctic sea and the mid- and high-latitude atmosphere. The components of the WAF are calculated according to Eq. (38) of Takaya and Nakamura (2001).

In this study, November is defined as early winter and DJ as middle winter. Monthly mean anomalies are calculated by the deviation from the long-term monthly mean climatology (1979/80--2015/16). In the following sections, 1979 refers to November--December 1979 and January 1980, and 1980 refers to November--December 1980 and January 1981, and so on. All the data used are detrended linearly, and thus intraseasonal and interannual variations are emphasized.

3. Results

3.1 *Reversal of the SH between November and DJ*

To capture the spatial phase relationships and the coherent variations between November and DJ SLP, firstly, the multivariate empirical orthogonal function (MV-EOF) analysis method (Wang, 1992) is employed. In this paper, a covariance matrix is constructed for the combined normalized November and DJ monthly averaged SLP to carry out the MV-EOF. The domain (10° --60° N, 60° --150° E), which includes most of Asia, is chosen for the analyses. The leading mode accounts for 26.42% of the total covariance for the November and DJ SLP together. The first mode exhibits an in-phase spatial pattern with consistent anomalies over most of central and eastern China and the entire tropics from November to DJ (figure omitted). Chang and Lu (2012) ascribed this mode to ENSO because of the significant correlations between this mode and the SST in the Niño3.4 region.

This study primarily focuses on the second empirical mode, which presents different spatial patterns between November and DJ and accounts for 14.04% of the total covariance. The SLP exhibits inverse signs in November and DJ in the mid--high latitudes (Figs. 2a and b). In November, the maximum amplitude lies to the northwest of Lake Balkhash, and the anomalies extend eastward to Northeast Asia. By contrast, the pattern in DJ shows nearly opposite anomalies over the analyzed domain. The maximum anomalies appear to the southeast of Lake Baikal and extend to southeastern China, which is in accordance with the aforementioned cold-air outbreak over East Asia associated with the SH. The second empirical mode displays large interannual variability, which can be seen through the second principal component (PC2) (Fig. 2c).

The SHI is applied to quantitatively describe the intensity of the reversion zone in Figs. 2a and b. Accordingly, the SHI in November and DJ are respectively referred to as SHI_N and SHI_DJ in the following. To further illustrate the atmospheric differences between November and DJ over the Eurasian continent, the regressions of SLP/SAT anomalies on the SHI from 1979 to 2015 are shown in Fig. 3. When the SHI_N is positive, significant positive SLP anomalies prevail in November north of 40° N and extend southeast to eastern China, Japan and the Northwest Pacific (Fig. 3a). Maximum amplitude appears in northwestern Siberia and adjacent areas, indicating prominent resemblance to the MV_EOF2 pattern in November. Correspondingly, anomalously low SAT appears in November to the west of Lake Baikal and stretches westward to the Caspian Sea, northeastward to the Far East, and southeastward to southern China (Fig. 3b). Interestingly, in the following DJ, noticeable positive anomalies replace those positive SLP (negative SAT) anomalies in November, although the anomalous area shrinks slightly and moves a little southward (Figs. 3c and d). These results further confirm the reversal of signals associated with the SH between November and DJ. Besides the simultaneous reflection, the impacts of November SH on the lagged atmospheric circulation anomalies are explored. The regressions of uv850, Z500 and u300 in DJ on the SHI_N are presented in Fig. 4. With the occurrence of a positive November SH, a significant anomalous cyclone (anticyclone) appears over Siberia (the West Pacific) during the following DJ, when anomalous southerly wind prevails along coastal East Asia (Fig. 4a). At 500 hPa, a meridional dipole of geopotential height anomalies (Fig. 4b), with significant negative anomalies throughout Siberia and positive anomalies expanding from the West Pacific to the hinterland

of Asia, indicates a weakening of both the Ural high and East Asian trough (He and Wang, 2013a). Meanwhile, the upper-tropospheric westerly jet stream decelerates over 30°--35°N, and a wide range of zonal wind accelerates to the north of the jet core (Fig. 4c). Thus, the meridional shear of zonal winds on the north side of the jet stream decreases, which results in a weaker EAWM and SH (Li and Yang, 2010). By contrast, when a weaker SH occurs in November, the EAWM-related circulation is more likely to be stronger in DJ. Overall, it is proved that the extratropical circulation processes in DJ over Siberia are negatively correlated with the preceding November SH.

In addition, Fig. 5 displays the time series of SHI_N and SHI_DJ during 1979--2015. The two indices barely keep the same phase with each other on the interannual timescale. During the 37-year period, more than half of the time (23 years) witnesses opposite relationships. To be specific, the correlation coefficient between SHI_N and SHI_DJ is −0.50 (above the 99% confidence level).

3.2 *Possible physical mechanisms*

The above analyses reveal the reversal of the SH between November and DJ. However, the underlying physical mechanism is not clear. As suggested by many previous studies (Thompson and Wallace, 2000; Wang and Ikeda, 2000; Gong et al., 2001), the SH is closely related to the AO. To examine the possible impact of the AO on the reversal of the SH, the November/DJ AO signal (obtained from the National Oceanic and Atmospheric Administration's website: https://www.esrl.noaa.gov/psd/data/correlation/ao.data) is removed from the November/DJ SLP via linear regression. The correlation coefficient between the

November and DJ non-AO SHI turns out to be −0.56 (above the 99% confidence level), indicating that the sign change between the SHI_N and SHI_DJ is unlikely due to the effect of the AO.

Jung et al. (2014) suggested that the involvement of subpolar processes may lead to more skillful forecasts than the midlatitude and tropical dynamics over eastern Europe and northern Asia, at least for medium-range and extended-range forecasts. Thus, it is important to connect the sub-seasonal variations of the SH to the Arctic change. Given the potential connection, regression maps of September and October sea-ice concentration on the SHI_N and SHI_DJ are presented in Fig. 6. The sea-ice concentration anomalies show high coherence from September to October with regard to SHI_N. Significant positive sea-ice concentration anomalies appear in the Kara Sea and the Laptev Sea in September (Fig. 6a) and persist into October (Fig. 6c). Besides, zonally elongated negative sea-ice concentration anomalies arise along the Siberian coast in September and October with regard to the SHI_DJ (Figs. 6b and d). The indication is that, when the SIA is reduced in September and October, the SH tends to be weaker in the subsequent November and stronger in DJ. Therefore, the following analyses mainly focus on the Arctic sea ice to explore the possible mechanism of the reversal of the SH between November and DJ. Following most earlier studies (Francis et al., 2009; Honda et al., 2009; Overland and Wang, 2010; Wu et al., 2011), we choose the September SIAI as representative of the autumn sea-ice variability. The normalized and detrended September SIAI is plotted in Fig. 5 along with SHI_N and SHI_DJ. There is a significant negative correlation (−0.42) between the SIAI and SHI_N and a significant positive correlation (0.49) between the

SIAI and SHI_DJ (both above the 99% confidence level). Moreover, during the 37 years of 1979--2015, 25 cases have opposite signs for the SIAI and SHI_N, while 23 cases have the same sign for the SIAI and SHI_DJ (the dots below in Fig. 5).

To better understand the influence of the autumn sea ice on the atmospheric circulation in the following winter, a composite analysis of the November/DJ SLP and Z500 anomalies between light and heavy sea-ice years is performed, based on a standard deviation of 0.5. In November, significant negative SLP anomalies can be seen throughout Siberia, with maximum amplitude of more than −5 hPa (Fig. 7a). The positive SLP anomalies during DJ show a significant positive anomaly center to the west of Siberia (Fig. 7b). The Z500 anomalies in November depict a hemispheric wave pattern resembling the wave-3 structure (Fig. 7c). By contrast, the 500 hPa anomalies display a dipole pattern over the Arctic-Eurasian sector in DJ (Fig. 7d). Considering the light sea ice in autumn, the DJ Z500 shows significant positive responses over northern Siberia and the adjacent Arctic sea, and negative responses over the midlatitude Asian continent, which bears some resemblance to the negative phase of the AO over the Arctic-Eurasian area (Tang et al., 2013; Mori et al., 2014).

The coupled interactions between the Arctic sea ice and the SHF, as well as the associated circulation anomalies in November and DJ are presented in Figs. 8a and b. Positive (negative) values of SHF are indicative of upward (downward) heat fluxes. The regressions of SHF are characterized by a sharp contrast over the Barents Sea. It is familiar that the reduction of sea ice (which means more open water) corresponds to increased ocean-to-atmosphere SHF (Honda et al., 2009). As open water has a lower albedo than ice, the surface ocean absorbs

more radiative energy during summertime (Perovich et al., 2007), and the growth of sea ice in November is hindered (Francis et al., 2009). Consequently, during November, the absorbed heat is transferred upward via turbulent fluxes, and the SHF exhibits significant positive anomalies in the Barents Sea and western Kara Sea (Fig. 8a). However, reversal appears in DJ with significant negative SHF anomalies (Fig. 8b). The downward SHF in absolute terms is larger in magnitude (~40 W m^{-2}) than the November upward SHF (~30 W m^{-2}). Results derived from ERA-Interim data (figure omitted) are consistent with those displayed in Fig. 8. Sorokina et al. (2016) demonstrated that the leading pattern of winter (here, December--February) interannual variability of turbulent heat flux over the Barents Sea is weakly correlated with sea ice. The ocean does no longer plays a dominant role in the ocean--atmosphere interaction; that is, the SHF anomalies are mainly driven by atmospheric changes in DJ. The warming of the overlying atmosphere due to Arctic amplification (Serreze and Barry, 2011) reduces the sea--air temperature differences, and thus the SHF is reduced (Sorokina et al., 2016).

Based on the above observational analyses, a physical mechanism that relates the autumn Arctic sea-ice loss to the reversal of the winter SH is investigated. Many previous studies have pointed out that the interaction between the storm track activity (also called the synoptic-scale eddy) and the low-frequency flow plays a key role in the variability of the atmospheric circulation (Lau and Nath, 1991; Hartmann and Lo, 1998; Hoskins, 2001; Grise et al., 2013; Lehmann and Coumou, 2015). Lau (1988) demonstrated that enhanced storm track activity is accompanied by westerly wind accelerating locally, as well as cyclonic vorticity forcing to the

north and anticyclonic vorticity forcing to the south, and vice versa. The modification of storm tracks can influence not only nearby areas but also downstream atmospheric circulation through synoptic transient eddy forcing (Tyrlis and Hoskins, 2008). In short-term climate change, the extratropical storm track plays an important role through transporting heat, moisture and momentum (Seierstad and Bader, 2008). Moreover, the increased temperature, moisture and the latent heating can enhance the eddy energy and storm track activity in a warmer climate (Hall et al., 1994). Previous analyses suggest that the change in surface heat flux over the Barents Sea is huge, so it is reasonable to associate sea-ice anomalies with storm tracks, as well as downstream intraseasonal circulation anomalies, which will be discussed next.

Figure 9 presents the regressions of storm track intensity and blocking frequency on the SIAI. The storm track activity is calculated as the variance of the 2.5--6-day bandpass-filtered Z250 ($\overline{(z')^2}$, where z' denotes the synoptic-scale geopotential height anomalies and the overbar indicates the time mean in November/DJ) (Lau and Nath, 1991). A blocking high event is defined if the daily Z500 exceeds one standard deviation above the monthly mean for each grid cell and persists for at least five consecutive days (Liu et al., 2012). The local blocking frequency for November (DJ) is measured by the ratio between the number of blocking days and the total number of days in November (DJ). Associated with reduced September SIA, increasing storm tracks appear over the Barents Sea coast and northeastern Europe in November (Fig. 9a) and significantly decreased storm tracks extend from eastern Europe southeastward to western Asia in DJ (Fig. 9b). Decreased blocking frequency is seen over the Urals in November (Fig. 9c) and, conversely, more extended increased blockings are seen over

the Urals and the Barents Sea in DJ (Fig. 9d), which is consistent with the circulation anomalies shown in Figs. 7 and 8. The zonal mean anomalies over the Eurasian region (20° --140° E) are further depicted in Fig. 10. In November, a smaller SIA favors the release of heat and moisture from the Arctic Ocean. Therefore, the static stability in the lower troposphere will decline and the baroclinicity aloft will be enhanced, which then intensify the storm track activity over the ocean and adjacent European continent (Figs. 9a and 10a). The wave activity propagates upward and equatorward at the latitude of the Arctic Ocean (65° --80° N), and then it propagates downward and diverges at 50° --65° N, which could result in the acceleration of westerly wind (Andrews et al., 1987). According to previous studies, positive storm track anomalies are accompanied by westerly wind anomalies and cyclonic vorticity forcing to their north (Lau, 1988; Gong et al., 2011; Chen et al., 2017). Correspondingly, large-scale cyclonic circulations prevail over high-latitude Eurasia (Fig. 8a). In DJ, in contrast, the upward SHF tightly related to the sea-ice loss disappears, with decreased heat and moisture supplies for the adjacent European region. Moreover, the meridional temperature gradient decreases because of the effect of the Arctic warming. The weakened meridional temperature gradient restrains the growth of baroclinic eddies and decelerates the westerlies (Fig. 10b). In this situation, the input of the westerly angular momentum is weakened over high-latitude Eurasia and less eddy energy is required to maintain the momentum balance (Held, 1993). Unsurprisingly, the transportation of wave activity from the Arctic to the region between 50° N and 65° N, which exists in November, disappears in DJ. In this latitudinal zone, in turn, a net loss of energy can be seen as the WAF diverges to lower latitudes. Finally, the intensity of

storm tracks decreases in DJ. To the north of the negative storm track anomalies, anticyclonic circulation anomalies replace the cyclonic winds prevailing in November (Fig. 8b). Notably, the distinct differences between November and DJ exist mostly in the troposphere.

Finally, the question as to the way that the SH responds to the variability of upstream storm tracks is resolved. Many studies have focused on this issue. For instance, Joung and Hitchman (1982) revealed a clear sequence whereby the surface synoptic situation over East Asia during wintertime is characterized by an intense eastward-moving perturbation beginning six or seven days in advance from the western North Atlantic across Eurasia. The synoptic-scale perturbations over Siberia share similar characteristics to the North Atlantic storm tracks (Hoskins and Hodges, 2002). By carrying out model experiments, Magnusdottir et al. (2004) confirmed that the December--March mean cold anomaly response appears in eastern Siberia when a weaker, southward-shifted, and more zonal storm track is found over the North Atlantic sector. More detailed mechanisms are documented as follows. When the North Atlantic--Europe storm tracks are active, the synoptic transient waves extending from the Atlantic to Europe intensify the anticyclonic wave breaking (Rivière and Orlanski, 2007; Zeng et al., 2015). Through the feedback of the transient waves on the monthly mean flow, the circumpolar eddy-driven jet is strengthened, and thus the southward movement of Arctic cold air is obstructed. The background field is disadvantageous for the maintenance of the Ural blocking high. As a result, the air over Siberia and East Asia becomes warmer and the SH becomes weaker, which shrinks and moves southward. The situation for DJ is basically reversed, and a stronger SH occurs. All these studies shed light on the impacts of upstream storm tracks on the SH and are

capable of proving that, under the condition of light autumn Arctic sea ice, the increased (decreased) storm track activity favors a weaker (stronger) SH in November (DJ).

In addition, the possible role of Siberian snow in the evolution of the SH during November and DJ is also investigated. As the Arctic sea ice is reduced, higher snow depth anomalies can be seen over most of the Eurasian land in DJ, especially in Siberia and northern China (Fig. 8d). The presence of an anomalously thick snow cover leads to near-surface cooling due to the high albedo of snow, which favors a strengthened and more expansive SH (Cohen and Entekhabi, 1999). However, there are barely any significant snow depth anomalies associated with low SIA in November (Fig. 8c). In particular, the northerly cold air advection along the eastern and southern flanks of the enhanced Ural high favors the thicker snowpack in DJ. Conversely, the warmer air advection from lower latitudes in November barely favor effective snow accumulation locally. Therefore, the large snowfall in DJ could further intensify the SH in DJ and enlarge the discrepancy of the SH in November and DJ.

3.3 *Validation by model simulations*

To test whether coupled models can represent the reversed response of the SH to autumn Arctic sea ice, we use the simulations (historical experiments) of five models [ACCESS1.0, ACCESS1.3, CESM1(CAM5), HadGEM2-CC, and GFDL CM2.1] from phase 5 of the Coupled Model Intercomparison Project (CMIP5) for the period 1979--2005. The selection of the CMIP5 models is primarily driven by their capability to reproduce the variability of observed sea-ice extent, SLP and uv850 fields since 1979 (e.g., Gleckler et al., 2008; Sperber et al., 2012; Liu et al., 2013). The available variables used include the monthly SLP, uv850,

Z500, sea-ice concentration, and surface snow amount. Before performing the analyses, we interpolate all the model simulation data to a horizontal resolution of 1°. Here, the ensemble mean results of the five model simulations are provided.

First, we calculate the correlation coefficient between SHI_N and SHI_DJ, which is −0.44 (above the 95% confidence level), based on the CMIP5 simulations during 1979--2004. Figure 11 illustrates the regression maps of the September and October ensemble-mean sea-ice concentration on the SHI_N and SHI_DJ. As expected, significant sea-ice anomalies persist from September to October along the Siberian coast with regard to either SHI_N or SHI_DJ, whereas an apparent reversal can be seen between the regressions upon SHI_N and SHI_DJ. The responses of Z500 and uv850 to the reduced Arctic sea ice are also shown in Fig. 12. The negative Z500 anomalies to the east of the Urals and the coherent cyclonic winds can be seen in November (Figs. 12a and c). Although the CMIP5-simulated anomalous amplitudes are smaller than observed, it is evident that the models simulate the dipole pattern of Z500 over the Arctic-Eurasian sector and anticyclonic winds over northern Europe in DJ (Figs. 12b and d), consistent with Figs. 7d and 8b. Moreover, no robust linkage between autumn sea ice and November snowfall in Siberia is found, but a significant increase in snow cover can be seen in DJ (Figs. 12c and d). To some extent, the physical linkages between autumn Arctic sea ice and the reversed SH in November and DJ can be reproduced by the historical simulations.

4. Summary and discussion

In this study, the impacts of autumn Arctic sea ice on the out-of-phase SH in November and DJ are investigated. The intensity of the SH is characterized by reversed anomalies between

November and DJ during the period 1979--2015, accompanied by reversed EAWM-related atmospheric circulation anomalies. The phenomenon of the SH reversal was proposed by Chang and Lu (2012), but the physical mechanisms were not clear. Our analyses propose a possible causal pathway by tracing the subseasonally varying SH to the preceding autumn sea-ice loss. It is illustrated that the November and DJ ocean-to-atmosphere heat flux exhibits opposite anomalies. When the autumn Arctic sea ice is light, in the ensuing November, through an eddy-mediated process and equatorward energy transportation, the baroclinic response to the thermal forcing of the positive SHF anomalies induces and facilitates the growth of storminess at mid--high latitudes. Thus, a significant strengthening of storm track activity is found across the Barents Sea and northeastern Europe in November. The analyses performed above are further supported by evidence provided by the findings of Kurita (2011) and Liu et al. (2012), which indicate that the Arctic Ocean is a major source of water vapor in northern (eastern) Europe in late autumn instead of December and subsequent winter months. Through the eddy--mean flow interaction, the Ural blocking high weakens, and thus the downstream SH becomes weaker. In the following DJ, in contrast with the November situation, the downward SHF anomalies and suppressed perturbation produce an unfavorable environment for storminess, such that a weaker storm track activity prevails and then a stronger SH appears. Moreover, the anomalously increased snowfall in Siberia could favor the strengthening of the SH in DJ. The associated dynamical processes in this study are summarized in Fig. 13 schematically.

Another point that should be noted is the reason why the SHF in DJ converts is not fully discussed. The weaker ocean-to-atmosphere SHF in DJ may be attributable to the leading role of the atmosphere in the air--sea interactions. The warming of the overlying air induces reduced sea--air and north--south temperature differences, which correspond with the negative SHF anomalies and easterly wind anomalies. From another perspective, the Arctic SIA anomalies in winter (here, December--February) perhaps cannot be considered simply as the persistence of the preceding autumn SIA anomalies (Tang et al., 2013). The winter sea-ice cover is likely to bear quite a bit of variability by itself, which is independent of the pre-existing autumn sea-ice anomalies. We believe that a consensus is looming, albeit further explorations are first needed.

The middle-winter (DJ) response in this study compares well with other studies using the DJF-mean winter signals. However, more often perceived as a transition month, November receives less attention in terms of atmospheric seasonal variations. In our study, of particular interest is the noticeable response in November, which is different from that in the ensuing DJ. During the transition seasons, although atmospheric internal variability is reduced, the eddy--mean flow interaction remains active and the forcing from SST anomalies tend to be largest (Kushnir et al., 2002). Knowledge of the extratropical atmosphere--ocean interaction during the transitional month is most likely to be useful in extended-range prediction. In this sense, if the relationship between the autumn Arctic sea ice and the SH reversal in November and DJ indicated in this study remains robust, we would expect to see a more changeable and complex winter-season climate in the near future as the sea-ice cover keeps diminishing.

Acknowledgments. This research was supported by the National Key R&D Program of China (Grant No. 2016YFA0600703), the National Natural Science Foundation of China (Grant Nos. 41505073 and 41605059), the Research Council of Norway–supported project SNOWGLACE (Grant No. 244166/E10), and the Young Talent Support Program of the China Association for Science and Technology (Grant No. 2016QNRC001). This study is also a contribution to the Bjerknes Centre for Climate Research, Bergen, Norway.

REFERENCES

Andrews, D. G., J. R. Holton., and C. B. Leovy, 1987: *Middle Atmosphere Dynamics*. Academic Press, 489 pp.

Castanheira, J. M., and H. F. Graf, 2003: North Pacific--North Atlantic relationships under stratospheric control? *J. Geophys. Res.*, **108**, 4036, https://doi.org/10.1029/2002JD002754.

Cattiaux, J., R. Vautard, C. Cassou, P. Yiou, V. Masson-Delmotte, and F. Codron, 2010: Winter 2010 in Europe: A cold extreme in a warming climate. *Geophys. Res. Lett.*, **37**, L20704, https://doi.org/10.1029/2010gl044613.

Chang, C. P., and M. M. Lu, 2012: Intraseasonal predictability of siberian high and east asian winter monsoon and its interdecadal variability. *J. Climate*, **25**, 1773--1778, https://doi.org/10.1175/jcli-d-11-00500.1.

Chen, S. F., R. G. Wu, and W. Chen, 2017: A strengthened impact of November Arctic oscillation on subsequent tropical Pacific sea surface temperature variation since the late-1970s. *Climate Dyn.*, **51**, 511--529, https://doi.org/10.1007/s00382-017-3937-x.

Cohen, J., and D. Entekhabi, 1999: Eurasian snow cover variability and Northern Hemisphere climate predictability. *Geophys. Res. Lett.*, **26**, 345--348, https://doi.org/10.1029/1998gl900321.

Cohen, J., and Coauthors, 2014: Recent Arctic amplification and extreme mid-latitude weather. *Nature Geoscience*, **7**, 627--637, https://doi.org/10.1038/ngeo2234.

Cohen, J., J. Jones, J. C. Furtado, and E. Tziperman, 2013: Warm Arctic, cold continents: A common pattern related to Arctic sea ice melt, snow advance, and extreme winter weather. *Oceanography*, **26**, 150--160, https://doi.org/10.5670/oceanog.2013.70.

Dee, D. P., and Coauthors, 2011: The ERA-Interim reanalysis: configuration and performance of the data assimilation system. *Quart. J. Roy. Meteor. Soc.*, **137**, 553--597, https://doi.org/10.1002/qj.828.

Deser, C., R. A. Tomas, and S. L. Peng, 2007: The transient atmospheric circulation response to north atlantic SST and sea ice anomalies. *J. Climate*, **20**, 4751--4767, https://doi.org/10.1175/jcli4278.1.

Ding, Y. H., 1990: Build-up, air mass transformation and propagation of Siberian high and its relations to cold surge in East Asia. *Meteor. Atmos. Phys.*, **44**, 281--292, https://doi.org/10.1007/BF01026822.

Ding, Y. H., and T. N. Krishnamurti, 1987: Heat budget of the Siberian high and the winter monsoon. *Mon. Wea. Rev.*, **115**, 2428--2449, https://doi.org/10.1175/1520-0493(1987)115<2428:HBOTSH>2.0.CO;2.

Francis, J. A., W. H. Chan, D. J. Leathers, J. R. Miller, and D. E. Veron, 2009: Winter Northern Hemisphere weather patterns remember summer Arctic sea-ice extent. *Geophys. Res. Lett.*, **36**, L07503, https://doi.org/10.1029/2009gl037274.

Gleckler, P. J., K. E. Taylor, and C. Doutriaux, 2008: Performance metrics for climate models. *J. Geophys. Res.*, **113**, D06104, https://doi.org/10.1029/2007jd008972.

Gong, D. Y., S. W. Wang, and J. H. Zhu, 2001: East Asian winter monsoon and arctic oscillation. *Geophys. Res. Lett.*, **28**, 2073--2076, https://doi.org/10.1029/2000GL012311.

Gong, D. Y., J. Yang, S. J. Kim, Y. Q. Gao, D. Guo, T. J. Zhou, M. and Hu, 2011: Spring Arctic Oscillation-East Asian summer monsoon connection through circulation changes over the western North Pacific. *Climate Dyn.*, **37**, 2199--2216, https://doi.org/10.1007/s00382-011-1041-1.

Grise, K. M., S. W. Son, and J. R. Gyakum, 2013: Intraseasonal and interannual variability in north american storm tracks and its relationship to equatorial pacific variability. *Mon. Wea. Rev.*, **141**, 3610--3625, https://doi.org/10.1175/mwr-d-12-00322.1.

Guirguis, K., A. Gershunov, R. Schwartz, and S. Bennett, 2011: Recent warm and cold daily winter temperature extremes in the Northern Hemisphere. *Geophys. Res. Lett.*, **38**, L17701, https://doi.org/10.1029/2011gl048762.

Hall, N. M. J., B. J. Hoskins, P. J. Valdes, and C. A. Senior, 1994: Storm tracks in a high-resolution GCM with doubled carbon dioxide. *Quart. J. Roy. Meteor. Soc.*, **120**, 1209--1230, https://doi.org/10.1002/qj.49712051905.

Hartmann, D. L., and F. Lo, 1998: Wave-driven zonal flow vacillation in the Southern Hemisphere. *J. Atmos. Sci.*, **55**, 1303--1315, https://doi.org/10.1175/1520-0469(1998)055<1303:WDZFVI>2.0.CO;2.

He, S. P., 2015: Asymmetry in the arctic oscillation teleconnection with January cold extremes in Northeast China. *Atmos. Oceanic Sci. Lett.*, **8**, 386--391, https://doi.org/10.3878/AOSL20150053.

He, S. P., and H. J. Wang, 2013a: Impact of the November/December Arctic Oscillation on the following January temperature in East Asia. *J. Geophys. Res.*, **118**, 12 981--12 998, https://doi.org/10.1002/2013jd020525.

He, S. P., and H. J. Wang, 2013b: Oscillating relationship between the East Asian Winter Monsoon and ENSO. *J. Climate*, **26**, 9819--9838, https://doi.org/10.1175/jcli-d-13-00174.1.

Held, I. M., 1993: Large-scale dynamics and global warming. *Bull. Amer. Meteor. Soc.*, **74**, 228--241, https://doi.org/10.1175/1520-0477(1993)074<0228:LSDAGW>2.0.CO;2.

Honda, M., J. Inoue, and S. Yamane, 2009: Influence of low Arctic sea-ice minima on anomalously cold Eurasian winters. *Geophys. Res. Lett.*, **36**, L08707, https://doi.org/10.1029/2008gl037079.

Hori, M. E., J. Inoue, T. Kikuchi, M. Honda, and Y. Tachibana, 2011: Recurrence of intraseasonal cold air outbreak during the 2009/2010 Winter in Japan and its ties to the atmospheric condition over the Barents-Kara Sea. *SOLA*, **7**, 25--28, https://doi.org/10.2151/sola.2011-007.

Hoskins, B. J., 2001: Modelling of the transient eddies and their feedback on the mean flow. *Large-Scale Dynamical Processes in the Atmosphere*. B. Hoskins and R. Pearce, Eds., Academic Press, 169 pp.

Hoskins, B. J., and K. I. Hodges, 2002: New perspectives on the Northern Hemisphere winter storm tracks. *J. Atmos. Sci.*, **59**, 1041--1061, https://doi.org/10.1175/1520-0469(2002)059<1041:NPOTNH>2.0.CO;2.

Huang, X. T., Y. N. Diao, and D. H. Luo, 2017: Amplified winter Arctic tropospheric warming and its link to atmospheric circulation changes. *Atmos. Oceanic Sci. Lett.*, **10**, 435--445, https://doi.org/10.1080/16742834.2017.1394159.

Inoue, J., M. E. Hori, and K. Takaya, 2012: The role of barents sea ice in the wintertime cyclone track and emergence of a warm-arctic cold-Siberian anomaly. *J. Climate*, **25**, 2561--2568, https://doi.org/10.1175/jcli-d-11-00449.1.

Joung, C. H., and M. H. Hitchman, 1982: On the role of successive downstream development in east asian polar air outbreaks. *Mon. Wea. Rev.*, **110**, 1224--1237, https://doi.org/10.1175/1520-0493(1982)110<1224:otrosd>2.0.co;2.

Jung, T., M. A. Kasper, T. Semmler, and S. Serrar, 2014: Arctic influence on subseasonal midlatitude prediction. *Geophys. Res. Lett.*, **41**, 3676--3680, https://doi.org/10.1002/2014gl059961.

Kalnay, E., and Coauthors, 1996: The NCEP/NCAR 40-year reanalysis project. *Bull. Amer. Meteor. Soc.*, **77**, 437--472, https://doi.org/10.1175/1520-0477(1996)077<0437:TNYRP>2.0.CO;2.

Kurita, N., 2011: Origin of Arctic water vapor during the ice-growth season. *Geophys. Res. Lett.*, **38**, L02709, https://doi.org/10.1029/2010gl046064.

Kushnir, Y., W. A. Robinson, I. Bladé, N. M. J. Hall, S. Peng, and R. Sutton, 2002: Atmospheric GCM response to extratropical SST anomalies: Synthesis and evaluation. *J. Climate*, **15**, 2233--2256, https://doi.org/10.1175/1520-0442(2002)015<2233:AGRTES>2.0.CO;2.

Lau, N. C., 1988: Variability of the observed midlatitude storm tracks in relation to low-frequency changes in the circulation pattern. *J. Atmos. Sci.*, **45**, 2718--2743, https://doi.org/10.1175/1520-0469(1988)045<2718:votoms>2.0.co;2.

Lau, N. C., and M. J. Nath, 1991: Variability of the baroclinic and barotropic transient eddy forcing associated with monthly changes in the midlatitude storm tracks. *J. Atmos. Sci.*, **48**, 2589--2613, https://doi.org/10.1175/1520-0469(1991)048<2589:VOTBAB>2.0.CO;2.

Lehmann, J., and D. Coumou, 2015: The influence of mid-latitude storm tracks on hot, cold, dry and wet extremes. *Scientific Reports*, **5**, 17491, https://doi.org/10.1038/srep17491.

Li, F., and H. J. Wang, 2013: Autumn sea ice cover, winter northern hemisphere annular mode, and winter precipitation in Eurasia. *J. Climate*, **26**, 3968--3981, https://doi.org/10.1175/jcli-d-12-00380.1.

Li, F., H. J. Wang, and Y. Q. Gao, 2015: Extratropical ocean warming and winter arctic sea ice cover since the 1990s. *J. Climate*, **28**, 5510--5522, https://doi.org/10.1175/jcli-d-14-00629.1.

Li, Y. Q., and S. Yang, 2010: A dynamical index for the East Asian winter monsoon. *J. Climate*, **23**, 4255--4262, https://doi.org/10.1175/2010jcli3375.1.

Liu, J. P., J. A. Curry, H. J. Wang, M. R. Song, and R. M. Horton, 2012: Impact of declining Arctic sea ice on winter snowfall. *Proceedings of the National Academy of Sciences of the United States of America*, **109**, 4074--4079, https://doi.org/10.1073/pnas.1114910109.

Liu, J. P., M. R. Song, R. M. Horton, and Y. Y. Hu, 2013: Reducing spread in climate model projections of a September ice-free Arctic. *Proceedings of the National Academy of Sciences of the United States of America*, **110**, 12 571—12 576, https://doi.org/10.1073/pnas.1219716110.

Magnusdottir, G., C. Deser, and R. Saravanan, 2004: The effects of North Atlantic SST and sea ice anomalies on the winter circulation in CCM3. Part I: Main features and storm track characteristics of the response. *J. Climate*, **17**, 857--876, https://doi.org/1520-0442(2004)017<0857:TEONAS>2.0.CO;2.

Mori, M., M. Watanabe, H. Shiogama, J. Inoue, and M. Kimoto, 2014: Robust Arctic sea-ice influence on the frequent Eurasian cold winters in past decades. *Nature Geoscience*, **7**, 869--873, https://doi.org/10.1038/ngeo2277.

Overland, J. E., K. R. Wood, and M. Y. Wang, 2011: Warm Arctic—cold continents: climate impacts of the newly open Arctic Sea. *Polar Research*, **30**, 15787, https://doi.org/10.3402/polar.v30i0.15787.

Overland, J. E., M. Wang, 2010: Large-scale atmospheric circulation changes are associated with the recent loss of Arctic sea ice. *Tellus A*: *Dynamic Meteorology and Oceanography*, **62**, 1--9, https://doi.org/10.1111/j.1600-0870.2009.00421.x.

Overland, J., J. A. Francis, R. Hall, E. Hanna, S. J. Kim, and T. Vihma, 2015: The melting arctic and midlatitude weather patterns: are they connected? *J. Climate*, **28**, 7917--7932, https://doi.org/10.1175/jcli-d-14-00822.1.

Park, T.-W., Ho, C.-H., and S. Yang, 2011: Relationship between the Arctic Oscillation and cold surges over East Asia. *J. Climate*, **24**, 68--83, https://doi.org/10.1175/2010JCLI3529.1.

Perovich, D. K., B. Light, H. Eicken, K. F. Jones, K. Runciman, and S. V. Nghiem, 2007: Increasing solar heating of the Arctic Ocean and adjacent seas, 1979--2005: Attribution and role in the ice-albedo feedback. *Geophys. Res. Lett.*, **34**, L19505, https://doi.org/10.1029/2007gl031480.

Rayner, N. A., D. E. Parker, E. B. Horton, C. K. Folland, L. V. Alexander, D. P. Rowell, E. C. Kent, and A. Kaplan, 2003: Global analyses of sea surface temperature, sea ice, and night marine air temperature since the late nineteenth century. *J. Geophys. Res.*, **108**, 4407, https://doi.org/10.1029/2002jd002670.

Rivière, G., and I. Orlanski, 2007: Characteristics of the Atlantic storm-track eddy activity and its relation with the North Atlantic Oscillation. *J. Atmos. Sci.*, **64**, 241--266, https://doi.org/10.1175/jas3850.1.

Ruggieri, P., R. Buizza, and G. Visconti, 2016: On the link between Barents-Kara sea ice variability and European blocking. *J. Geophys. Res.*, **121**, 5664--5679, https://doi.org/10.1002/2015jd024021.

Seierstad, I. A., and J. Bader, 2008: Impact of a projected future Arctic Sea Ice reduction on extratropical storminess and the NAO. *Climate Dyn.*, **33**, 937--943, https://doi.org/10.1007/s00382-008-0463-x.

Serreze, M. C., and R. G. Barry, 2011: Processes and impacts of Arctic amplification: A research synthesis. *Global and Planetary Change*, **77**, 85--96, https://doi.org/10.1016/j.gloplacha.2011.03.004.

Sorokina, S. A., C. Li, J. J. Wettstein, and N. G. Kvamstø, 2016: Observed atmospheric coupling between barents sea ice and the Warm-Arctic Cold-Siberian anomaly pattern. *J. Climate*, **29**, 495--511, https://doi.org/10.1175/jcli-d-15-0046.1.

Sperber, K. R., H. Annamalai, I. S. Kang, A. Kitoh, A. Moise, A. Turner, B. Wang, and T. Zhou, 2012: The Asian summer monsoon: an intercomparison of CMIP5 vs. CMIP3 simulations of the late 20th century. *Climate Dyn.*, **41**, 2711--2744, https://doi.org/10.1007/s00382-012-1607-6.

Takaya, K., and H. Nakamura, 2001: A formulation of a phase-independent wave-activity flux for stationary and migratory quasigeostrophic eddies on a zonally varying basic flow. *J. Atmos. Sci.*, **58**, 608--627, https://doi.org/10.1175/1520-0469(2001)058<0608:AFOAPI>2.0.CO;2.

Takaya, K., and H. Nakamura, 2005a: Geographical dependence of upper-level blocking formation associated with intraseasonal amplification of the siberian high. *J. Atmos. Sci.*, **62**, 4441--4449, https://doi.org/10.1175/JAS3628.1.

Takaya, K., and H. Nakamura, 2005b: Mechanisms of intraseasonal amplification of the cold siberian high. *J. Atmos. Sci.*, **62**, 4423--4440, https://doi.org/10.1175/JAS3629.1.

Tang, Q. H., X. J. Zhang, X. H. Yang, and J. A. Francis, 2013: Cold winter extremes in northern continents linked to Arctic sea ice loss. *Environmental Research Letters*, **8**, 014036, https://doi.org/10.1088/1748-9326/8/1/014036.

Thompson, D. W. J., and J. M. Wallace, 1998: The Arctic oscillation signature in the wintertime geopotential height and temperature fields. *Geophys. Res. Lett.*, **25**, 1297--1300, https://doi.org/10.1029/98gl00950.

Thompson, D. W. J., and J. M. Wallace, 2000: Annular modes in the extratropical circulation. Part I: Month-to-month variability. *J. Climate*, **13**, 1000--1016, https://doi.org/10.1175/1520-0442(2000)013<1000:amitec>2.0.co;2.

Tyrlis, E., and B. J. Hoskins, 2008: Aspects of a Northern hemisphere atmospheric blocking climatology. *J. Atmos. Sci.*, **65**, 1638--1652, https://doi.org/10.1175/2007jas2337.1.

Wang, B., 1992: The vertical structure and development of the ENSO anomaly mode during 1979-1989. *J. Atmos. Sci.*, **49**, 698--712, https://doi.org/10.1175/1520-0469(1992)049<0698:TVSADO>2.0.CO;2.

Wang, H. J., and S. P. He, 2012a: The increase of snowfall in Northeast China after the mid-1980s. *Chinese Science Bulletin*, **58**, 1350--1354, https://doi.org/10.1007/s11434-012-5508-1.

Wang, H. J., and S. P. He, 2012b: Weakening relationship between East Asian winter monsoon and ENSO after mid-1970s. *Chinese Science Bulletin*, **57**, 3535--3540, https://doi.org/10.1007/s11434-012-5285-x.

Wang, J., and M. Ikeda, 2000: Arctic oscillation and Arctic sea-ice oscillation. *Geophys. Res. Lett.*, **27**, 1287--1290, https://doi.org/10.1029/1999gl002389.

Wegmann, M., and Coauthors, 2015: Arctic moisture source for Eurasian snow cover variations in autumn. *Environmental Research Letters*, **10**, 054015, https://doi.org/10.1088/1748-9326/10/5/054015.

Wu, B. Y., and J. Wang, 2002: Winter arctic oscillation, Siberian high and east asian winter monsoon. *Geophys. Res. Lett.*, **29**, 1897, https://doi.org/10.1029/2002gl015373.

Wu, B. Y., J. Z. Su, and R. H. Zhang, 2011: Effects of autumn-winter Arctic sea ice on winter Siberian High. *Chinese Science Bulletin*, **56**, 3220--3228, https://doi.org/10.1007/s11434-011-4696-4.

Wu, B. Y., K. Yang, and J. A. Francis, 2017: A cold event in asia during January--February 2012 and its possible association with Arctic Sea ice loss. *J. Climate*, **30**, 7971--7990, https://doi.org/10.1175/jcli-d-16-0115.1.

Wu, Q. G., and X. D. Zhang, 2010: Observed forcing-feedback processes between Northern Hemisphere atmospheric circulation and Arctic sea ice coverage. *J. Geophys. Res.*, **115**, D14119, https://doi.org/10.1029/2009jd013574.

Zeng, D. W., W. J. Zhu, X. J. Ma, P. S. Gu, M. Y. Liu, and J. Gao, 2015: North Atlantic storm track and its infulence on Siberian High in winter. *Transactions of Atmospheric Sciences*, **38**, 232--240, https://doi.org/10.13878/j.cnki.dqkxxb.20121003001. (in Chinese)

Zhao, P., and R. H. Zhang, 2006: Relationship of interannual variation between an eastern Asia- pacific dipole pressure pattern and East Asian monsoon. *Chinese Journal of Atmospheric Sciences*, **30**, 307--316.

Zhou, W., 2017: Impact of Arctic amplification on East Asian winter climate. *Atmospheric and Oceanic Science Letters*, **10**, 385--388, https://doi.org/10.1080/16742834.2017.1350093.

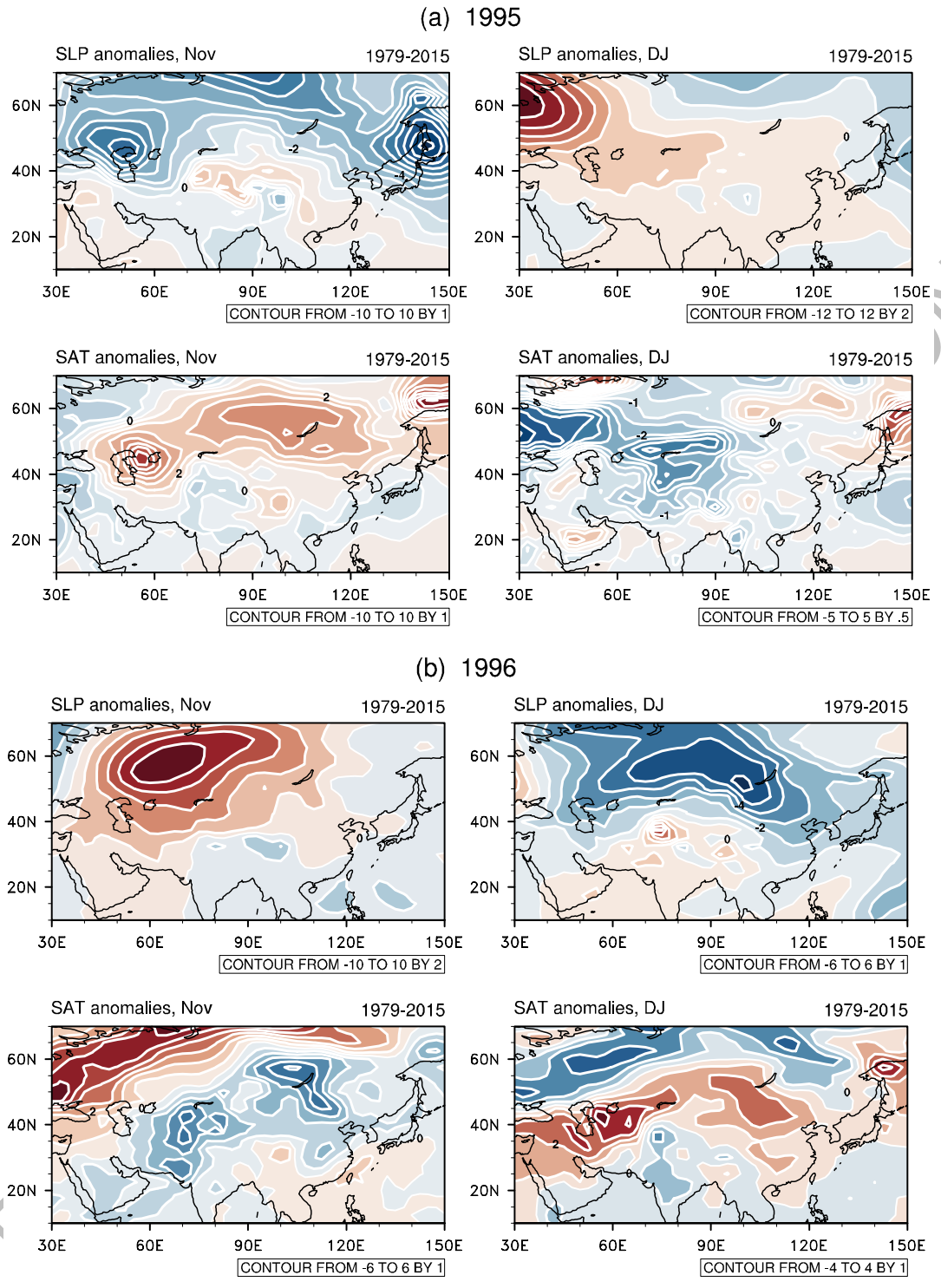

Fig. 1. SLP anomalies (top; units: hPa) and SAT anomalies (bottom; units: K) in November (left) and DJ (right) in (a) 1995 and (b) 1996. Anomalies are calculated based on the climatology of 1979--2015.

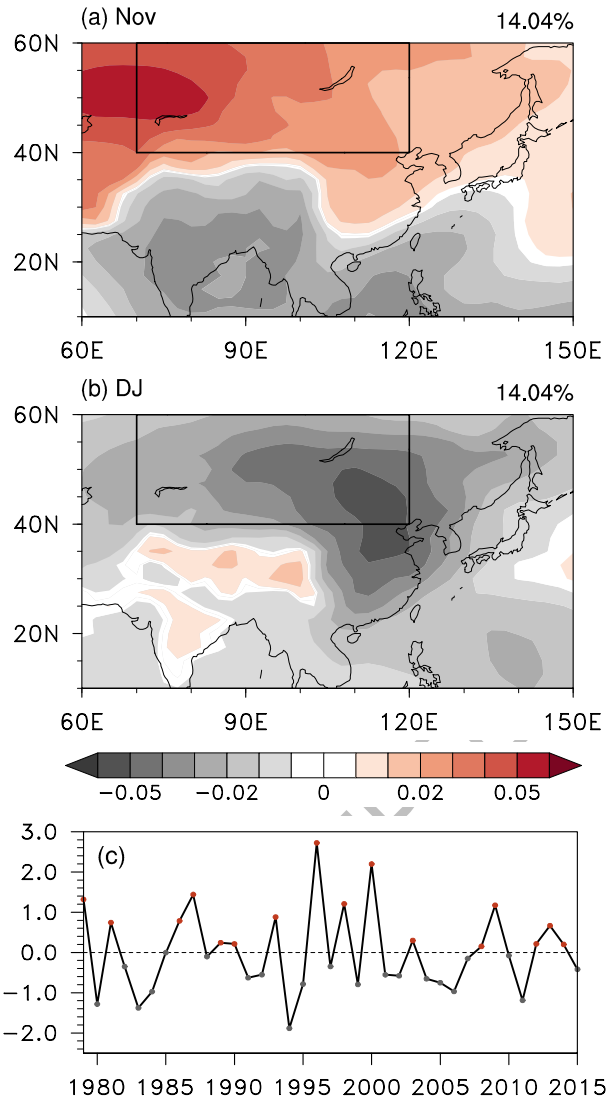

Fig. 2. Spatial patterns of the second MV-EOF modes of (a) November and (b) DJ SLP. (c) Normalized time series of the second principal component (PC2). The region where the SHI is calculated is denoted by the black rectangular frame in panels (a, b).

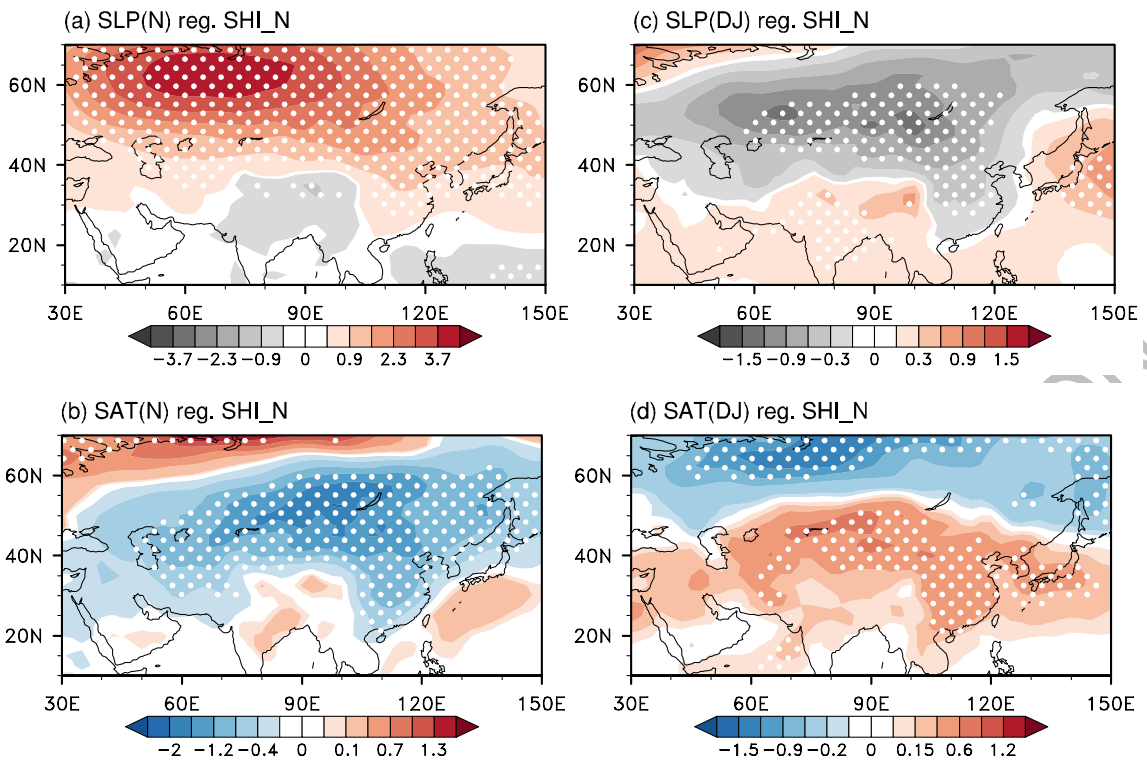

Fig. 3. Regressions of November (a) SLP (units: hPa) and (b) SAT (units: K) anomalies on the SHI_N during 1979--2015. Panels (c, d) are similar to (a, b), respectively, except that they show the SLP and SAT in DJ. Dotted regions indicate the anomalies significant at the 90% confidence level, based on a two-tailed Student's *t*-test.

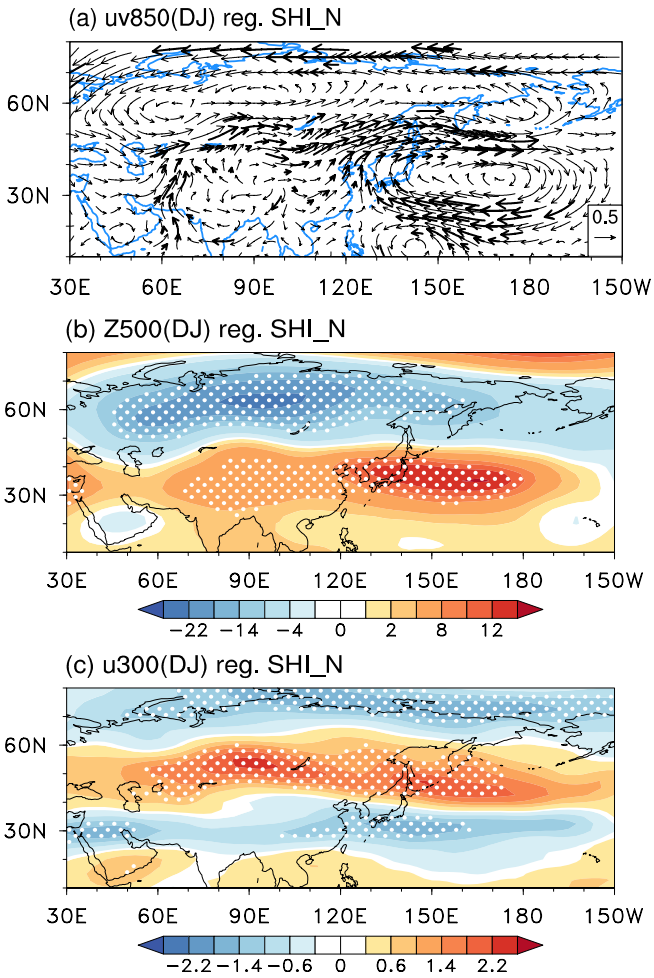

Fig. 4. Regressions of (a) wind at 850 hPa (units: m s^{-1}), (b) geopotential height at 500 hPa (units: gpm), and (c) zonal wind at 300 hPa (units: m s^{-1}) in DJ on the SHI_N. Bold arrows in (a) indicate either component of the wind anomalies is significant at the 90% confidence level. Dotted regions in (b, c) indicate anomalies significant at the 90% confidence level, based on a two-tailed Student's *t*-test.

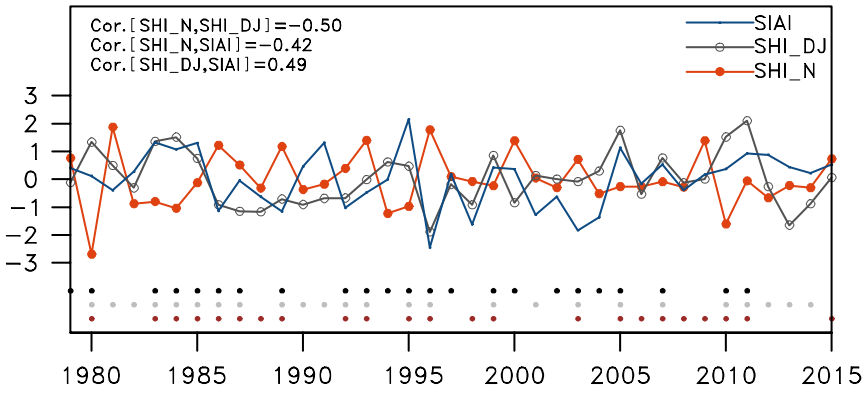

Fig. 5. Normalized and detrended time series of the SIAI in September, along with the SHI_DJ and SHI_N during 1979--2015. The black (grey) dots in the bottom panel indicate the years when the SHI_N and SHI_DJ (SHI_N and SIAI) are in reverse phase, and the brown dots indicate the years when the SHI_DJ and SIAI are in the same phase.

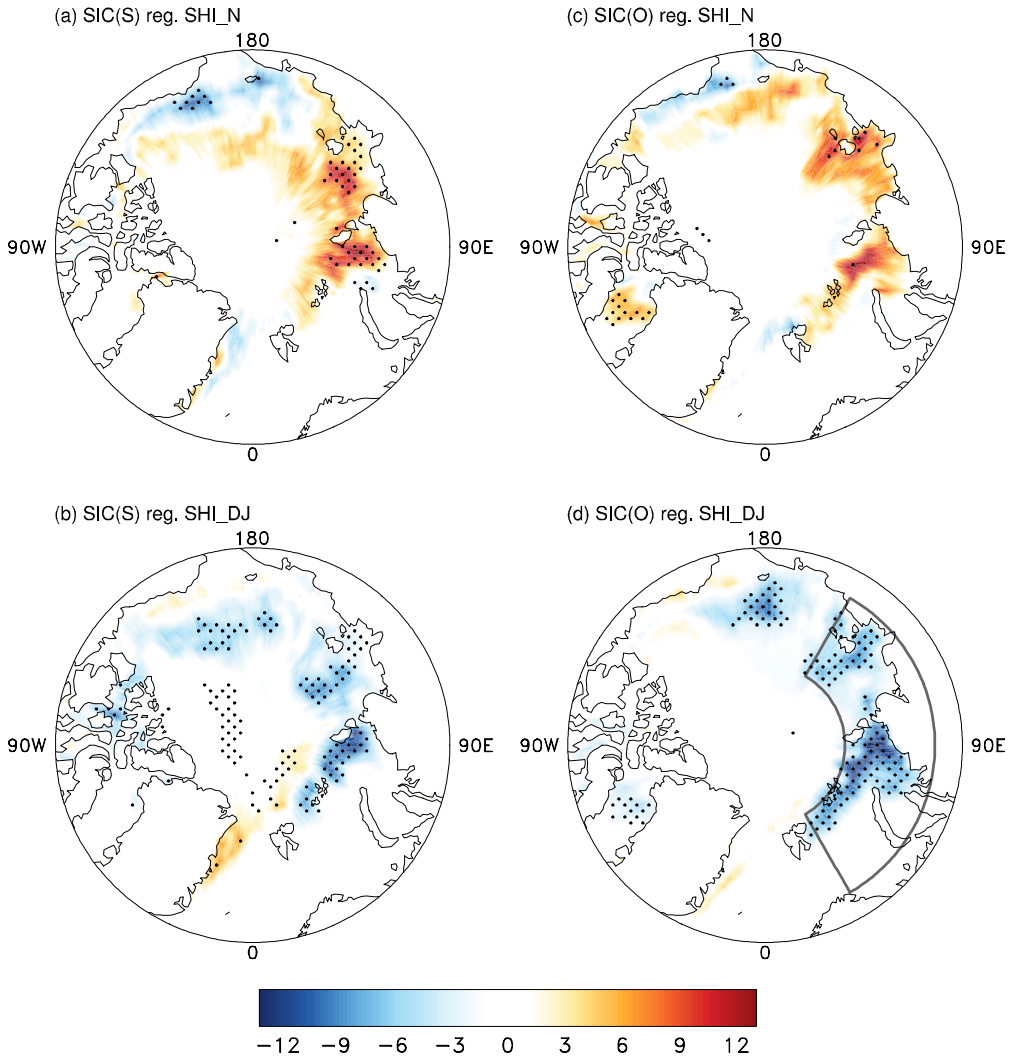

Fig. 6. Regressions of September sea-ice concentration (SIC) anomalies (units: %) on the (a) SHI_N and (b) SHI_DJ. Panels (c, d) are similar to (a, b), respectively, except they show the October SIC anomalies. Dotted regions indicate anomalies significant at the 90% confidence level, based on a two-tailed Student's *t*-test. The region for the definition of the SIAI is denoted in panel (d).

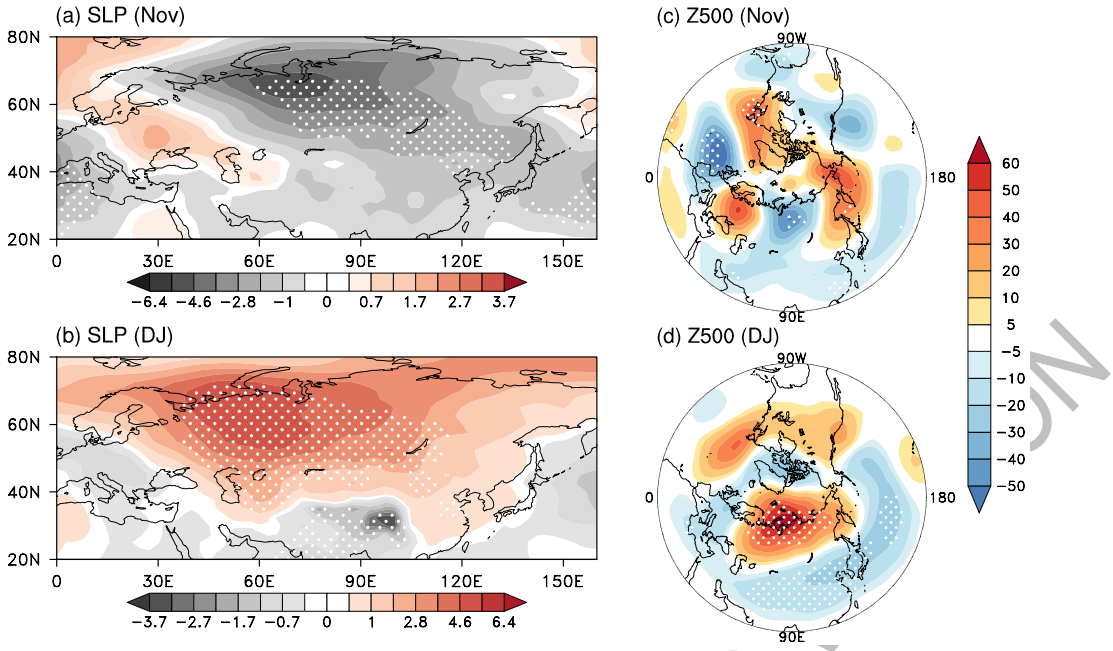

Fig. 7. Composite differences of SLP (units: hPa) in (a) November and (b) DJ between the years of positive and negative September SIAI. Panels (c, d) are similar to (a, b), respectively, except they show the Z500 anomalies (units: gpm). Dotted regions indicate anomalies significant at the 90% confidence level, based on a two-tailed Student's *t*-test.

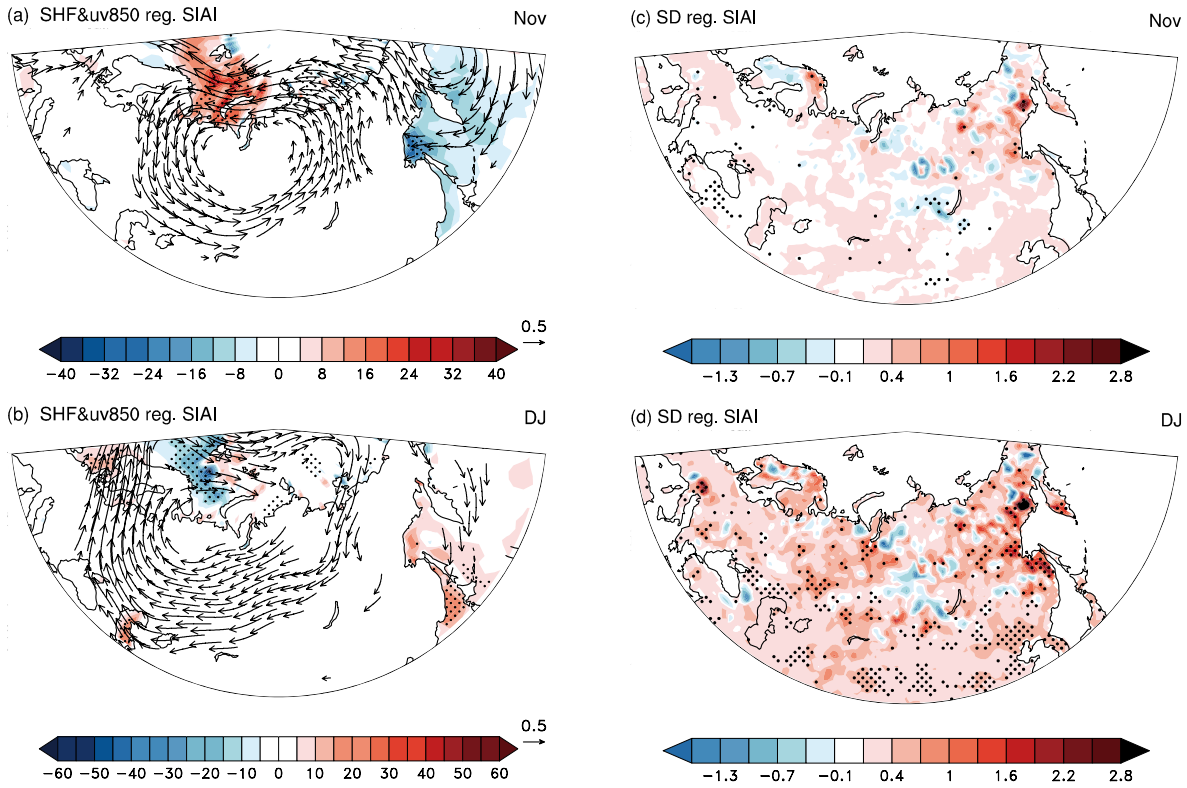

Fig. 8. Regressions of November (a) SHF (shading; units: W m^{-2}) and 850 hPa winds (vectors; units: m s^{-1}), and (c) snow depth (SD) anomalies (units: cm), on the SIAI. Positive SHF anomalies indicate anomalous upward fluxes. Panels (b, d) are similar to (a, c), respectively, except for DJ. Winds where either component of the wind anomaly exceeds 0.3 m s^{-1} are displayed. Dotted regions indicate anomalies significant at the 90% confidence level, based on a two-tailed Student's *t*-test.

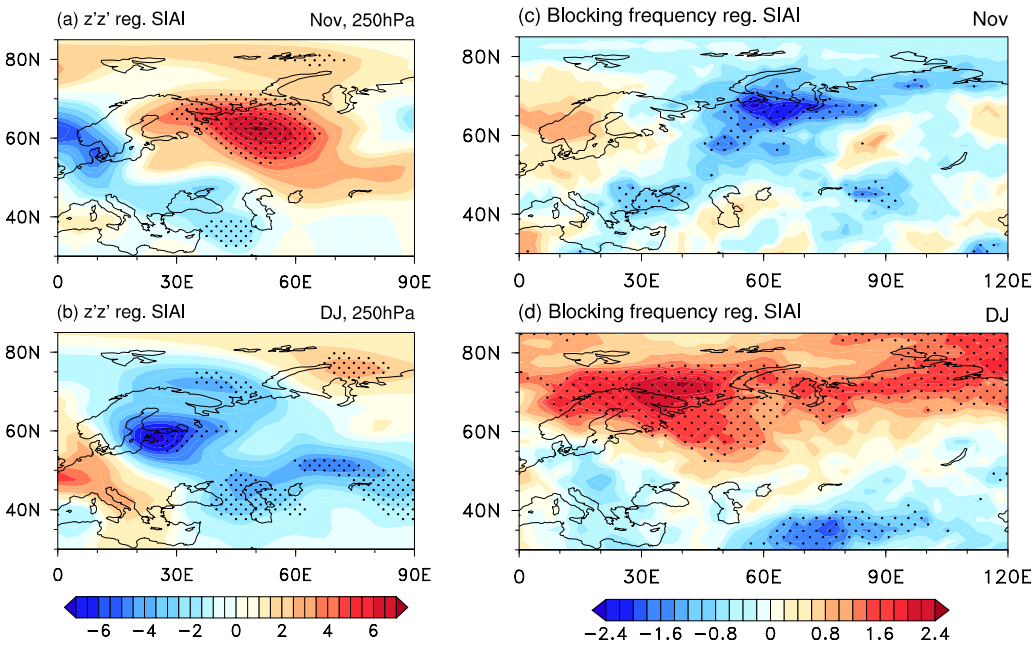

Fig. 9. Regressions of November (a) mean storm track intensity (units: dgpm^2) and (c) blocking frequency (units: %) on the SIAI. Panels (b, d) are similar to (a, c), respectively, except for DJ. Dotted regions indicate anomalies significant at the 90% confidence level, based on a two-tailed Student's *t*-test.

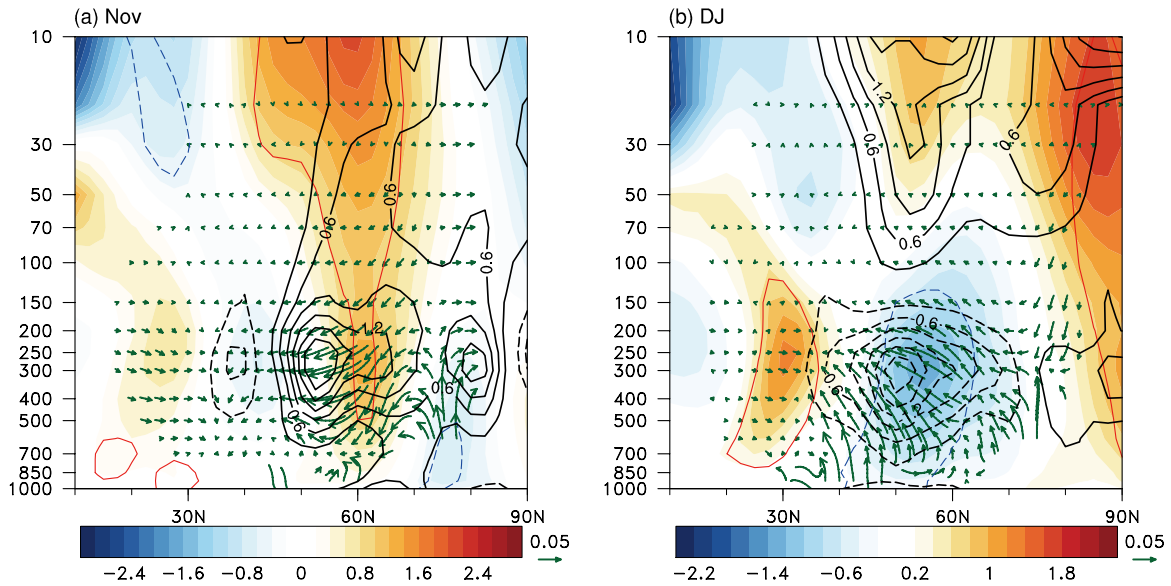

Fig. 10. Regressions of zonal wind (shading; units: m s^{-1}), WAF (vectors; units: m^2 s^{-2}) and storm track intensity (black contours; units: $dgpm^2$) averaged between 20°E and 140°E in (a) November and (b) DJ on the SIAI. The vertical component of the WAF is multiplied by 125 (Castanheira and Graf, 2003). Red and blue contours indicate zonal wind anomalies significant at the 90% confidence level, based on a two-tailed Student's *t*-test.

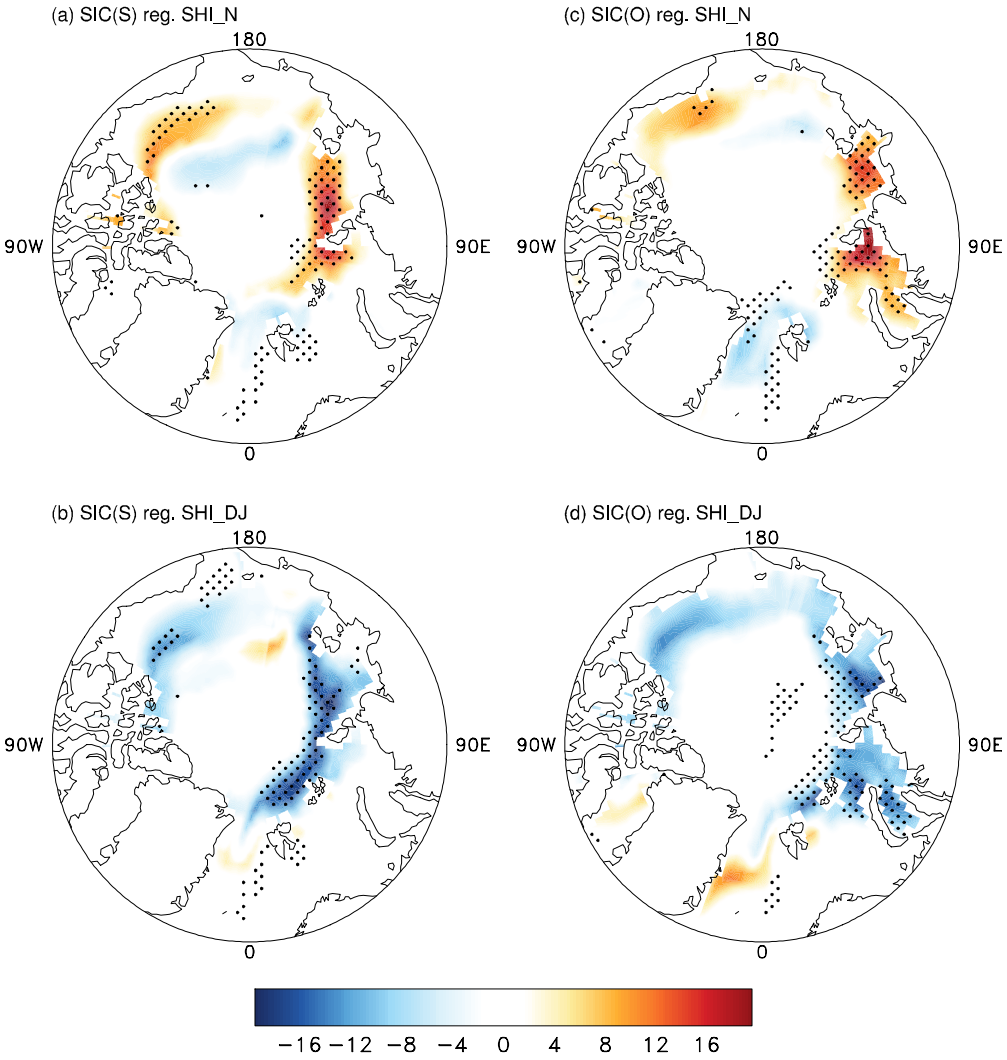

Fig. 11. As in Fig. 6, except for CMIP5 historical simulations (1979--2004).

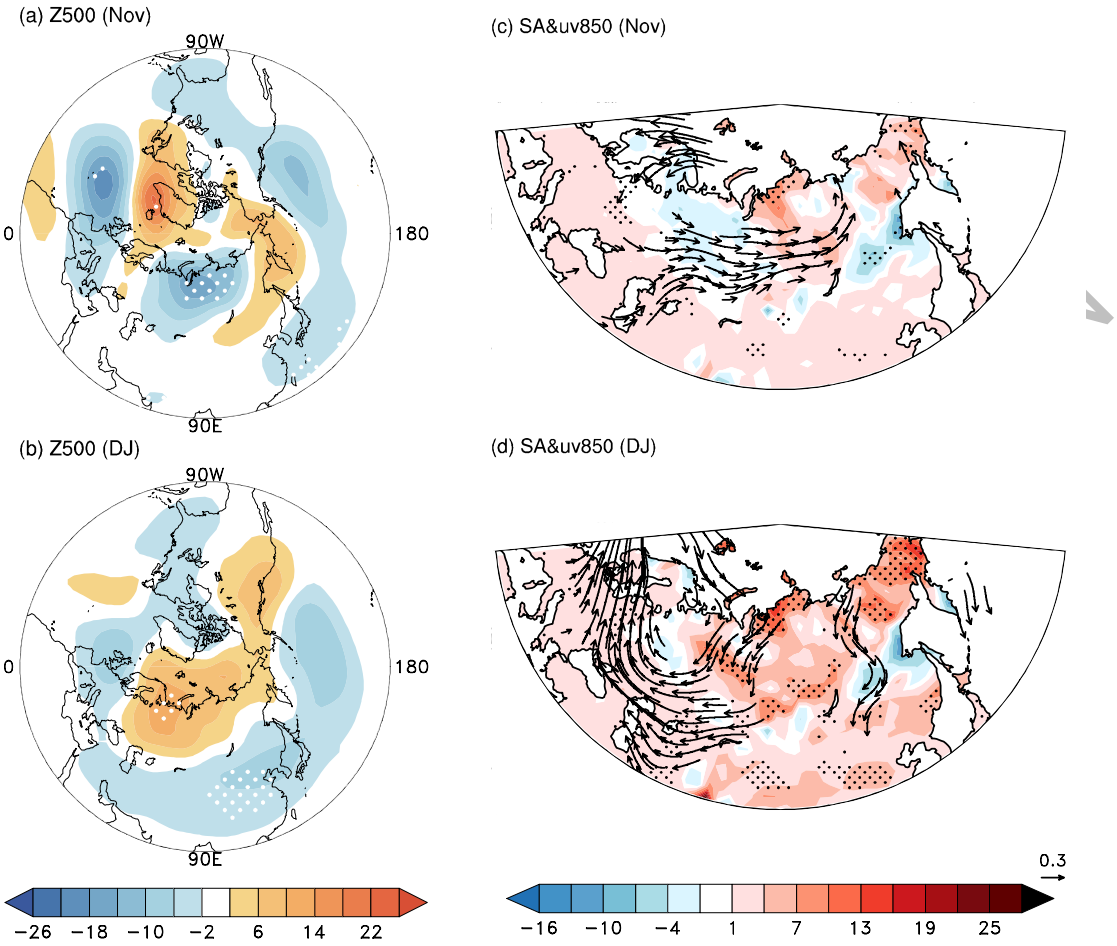

Fig. 12. Composite differences of Z500 anomalies (units: gpm) in (a) November and (b) DJ between the years of positive and negative SIAI; regressions of (c) November and (d) DJ surface snow amount (SA) (shading; units: kg m^{-2}) and 850 hPa winds (vectors; units: m s^{-1}) anomalies on the SIAI, during 1979--2004, derived from the CMIP5 historical simulations. Winds where either component of the wind anomaly exceeds 0.15 m s^{-1} are displayed. Dotted regions indicate anomalies significant at the 90% confidence level, based on a two-tailed Student's *t*-test.

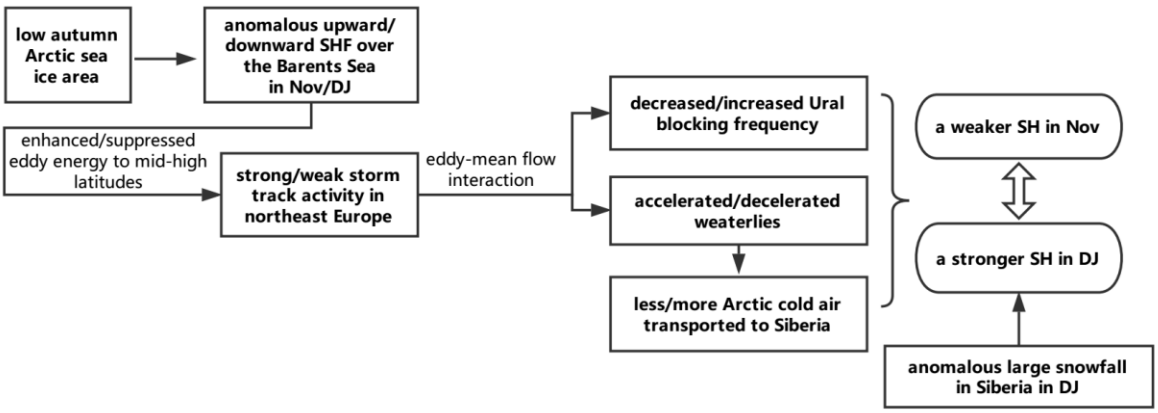

Fig. 13. Schematic diagram illustrating the mechanisms for the low autumn Arctic sea ice leading to the reversal of the SH in November and DJ.